Journal of the Physical Society of Japan
Vol. 67, No. 8, August, 1998, pp. 2857–2862

Berry's Phase and Absence of Back Scattering in Carbon Nanotubes

Tsuneya ANDO, Takeshi NAKANISHI,[1] and Riichiro SAITO[2]

Institute for Solid State Physics, University of Tokyo
7–22–1 Minato-ku, Roppongi, Tokyo 106

[1] *The Institute of Physical and Chemical Research (RIKEN)*
2–1 Hirosawa, Wako-shi, Saitama 351-01

[2] *Department of Electronics Engineering*
University of Electro-Communications, Chofugaoka, Chofu, Tokyo 182

(Received March 16, 1998)

The absence of back scattering in carbon nanotubes is shown to be ascribed to Berry's phase which corresponds to a sign change of the wave function under a spin rotation of a neutrino-like particle in a two-dimensional graphite. Effects of trigonal warping of the bands appearing in a higher order $\boldsymbol{k}\cdot\boldsymbol{p}$ approximation are shown to give rise to a small probability of back scattering.

KEYWORDS: graphite, carbon nanotube, fullerene tube, effective-mass theory, impurity scattering, Berry's phase

§1. Introduction

A carbon nanotube (CN) consists of coaxially rolled graphite sheets.[1)] Because the distance between different sheets is much larger than the distance between the nearest neighbor carbon atoms, electronic properties of CN's are determined essentially by those of a single-shell CN. A single-shell CN can be either a metal or a semiconductor depending on the circumference length and the helical fashion. The purpose of this paper is to clarify the origin of the absence of back scattering for scatterers having a potential range comparable to or larger than the lattice constant, predicted previously.[2)]

Various calculations have been performed to understand energy bands of CN's.[3−13)] The characteristic properties are all reproduced quite well in a $\boldsymbol{k}\cdot\boldsymbol{p}$ method.[14,15)] It has been successful in the study of magnetic properties including the Aharonov-Bohm (AB) effect on the band gap,[16,17)] optical absorption spectra,[18−20)] and lattice instabilities in the presence and absence of a magnetic field.[21,22)]

Transport properties of CN's are interesting because of their unique topological structure. There have been some reports on experimental study of transport in CN bundles.[23)] Measurements of magnetotransport of a single nanotube became possible.[24,25)] Tunneling probabilities at a finite-length CN[26)] and a connection of different CN's[27−30)] were calculated. The conductivity was calculated also in a constant-relaxation-time approximation in the absence of a magnetic field.[31)] The magnetoconductivity was calculated using the Boltzmann transport equation[32)] and in a transmission approach[33)] for a model of short-range scatterers.

In a previous paper,[2)] effects of impurity scattering in CN's were studied in detail and a possibility of complete absence of back scattering was pointed out and proved rigorously except for scatterers having a potential range smaller than the lattice constant. In this paper we shall relate this intriguing fact to Berry's phase acquired by a rotation in the wave vector space in the system described by a $\boldsymbol{k}\cdot\boldsymbol{p}$ Hamiltonian which is the same as that of a neutrino satisfying Weyl's equation. Effects of trigonal warping of the bands appearing in a higher order $\boldsymbol{k}\cdot\boldsymbol{p}$ approximation are studied also.

§2. Effective-Mass Equation

The lattice structure of a two-dimensional (2D) graphite and corresponding first Brillouin zone are shown in Fig. 1. A unit cell contains two carbon atoms denoted as A and B. The coordinate system (x', y') is fixed onto the graphite sheet (x' is in the direction of $\boldsymbol{a}$ with $a=|\boldsymbol{a}|$ being the lattice constant) and (x, y) is chosen in such a way that the x axis is in the chiral direction of CN, i.e., the direction along the circumference, and the y axis in the direction of the axis. The angle between the x and x' direction is called a chiral angle and denoted as η. We have $\eta=0$ for a zig-zag nanotube and $\eta=\pi/6$ for an armchair nanotube. The conduction and valence bands of 2D graphite cross each other at K and K' points where the bands have approximately a linear dispersion as a function of the wave vector. The K and K' points are located at a corner of the boundary of the first Brillouin zone and are not equivalent.

In the effective-mass approximation, the electronic states of a 2D graphite near a K point are described by a $\boldsymbol{k}\cdot\boldsymbol{p}$ equation as[34)]

$$\gamma\,(\vec{\sigma}\cdot\hat{\boldsymbol{k}})\,\boldsymbol{F}(\boldsymbol{r})=\varepsilon\,\boldsymbol{F}(\boldsymbol{r}), \tag{2.1}$$

or

$$\gamma\begin{pmatrix}0 & \hat{k}_x-\mathrm{i}\hat{k}_y\\ \hat{k}_x+\mathrm{i}\hat{k}_y & 0\end{pmatrix}\begin{pmatrix}F_A(\boldsymbol{r})\\ F_B(\boldsymbol{r})\end{pmatrix}=\varepsilon\begin{pmatrix}F_A(\boldsymbol{r})\\ F_B(\boldsymbol{r})\end{pmatrix}, \tag{2.2}$$

where γ is the band parameter, $\vec{\sigma}=(\sigma_x,\sigma_y)$ is the Pauli

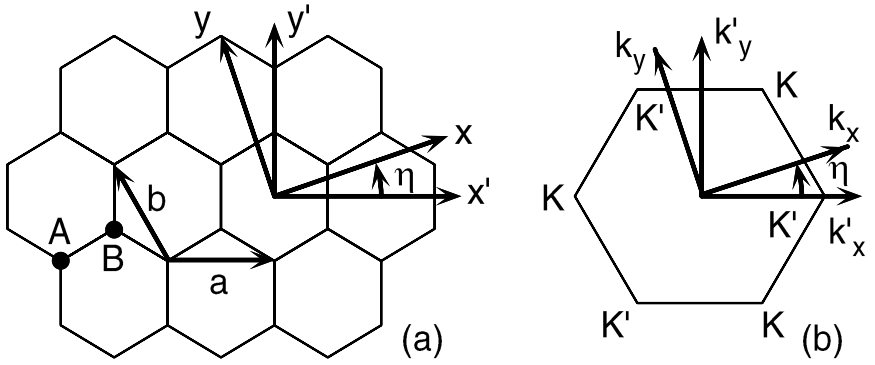

Fig. 1 Lattice structure and first Brillouin zone of a two-dimensional graphite. The coordinate system (x', y') is fixed onto the graphite sheet and (x, y) is chosen in such a way that the x axis is in the circumference direction of CN and y in the axis direction. The chiral angle is denoted as η. A unit cell contains two carbon atoms denoted as A and B. The corner points K and K' of the Brillouin zone are not equivalent.

spin matrix, $\hat{\boldsymbol{k}} = (\hat{k}_x, \hat{k}_y)$ is a wave vector operator defined by $\hat{\boldsymbol{k}} = -\mathrm{i}\vec{\nabla}$, and F_A and F_B represent the amplitude of the envelope functions at A and B carbon atoms, respectively. The eigen wave functions and energies of this Hamiltonian are written as

$$\boldsymbol{F}_{s\boldsymbol{k}}(\boldsymbol{r}) = \frac{1}{\sqrt{LA}} \exp(\mathrm{i}\boldsymbol{k}\cdot\boldsymbol{r})\, \boldsymbol{F}_{s\boldsymbol{k}}, \tag{2.3}$$

$$\varepsilon_s(\boldsymbol{k}) = s\gamma|\boldsymbol{k}|, \tag{2.4}$$

where L is the circumference of CN, A is the length, and $s = +1$ and -1 denote conduction and valence bands, respectively. In metallic CN's the wave vector in the k_x direction is quantized into $k_x = \kappa(n)$ with $\kappa(n) = 2\pi n/L$ where n is an integer. In general, we can write eigenvector $\boldsymbol{F}_{s\boldsymbol{k}}$ as

$$\boldsymbol{F}_{s\boldsymbol{k}} = \exp[\mathrm{i}\phi_s(\boldsymbol{k})]\, R^{-1}[\theta(\boldsymbol{k})]\, |s), \tag{2.5}$$

where $\phi_s(\boldsymbol{k})$ is an arbitrary phase factor, $\theta(\boldsymbol{k})$ is the angle between wave vector $\boldsymbol{k}$ and the k_y axis, i.e., $k_x + \mathrm{i}k_y = \mathrm{i}|\boldsymbol{k}|\mathrm{e}^{\mathrm{i}\theta(\boldsymbol{k})}$, $R(\theta)$ is a spin-rotation operator, given by

$$R(\theta) = \exp\left(\mathrm{i}\frac{\theta}{2}\sigma_z\right) = \begin{pmatrix} \exp(+\mathrm{i}\theta/2) & 0 \\ 0 & \exp(-\mathrm{i}\theta/2) \end{pmatrix}, \tag{2.6}$$

with σ_z being a Pauli matrix, and $|s)$ is the eigenvector for the state with $\boldsymbol{k}$ in the positive k_y direction, given by

$$|s) = \frac{1}{\sqrt{2}} \begin{pmatrix} -\mathrm{i}s \\ 1 \end{pmatrix}. \tag{2.7}$$

Obviously, we have

$$R(\theta_1)R(\theta_2) = R(\theta_1+\theta_2), \quad R(-\theta) = R^{-1}(\theta), \quad \text{etc.} \tag{2.8}$$

Further, because $R(\theta)$ describes the rotation of a spin, it has the property

$$R(\theta \pm 2\pi) = -R(\theta), \tag{2.9}$$

which gives $R(-\pi) = -R(+\pi)$. In order to define states and corresponding wave functions uniquely, we shall assume in the following that

$$-\pi < \theta(\boldsymbol{k}) \le +\pi. \tag{2.10}$$

By choosing the phase $\phi_s(\boldsymbol{k})$ in an appropriate manner, the wave function can be chosen as either continuous or discontinuous across the point corresponding to $\theta = +\pi$ and $-\pi$ in the $\boldsymbol{k}$ space. The results are certainly independent of such choices.

§3. Absence of Back Scattering

In the following we shall consider a back scattering process $\boldsymbol{k} \to -\boldsymbol{k}$ due to an arbitrary external potential having a range larger than or comparable to the lattice constant in a 2D graphite sheet, where $\boldsymbol{k} = (0, k)$. Only difference arising in nanotubes is discretization of the wave vector in the k_x direction as mentioned above. We shall confine ourselves to states in the vicinity of the K point, but the extension to states near a K' point is straightforward. Introduce a T matrix defined by

$$T = V + V\frac{1}{\varepsilon - \mathcal{H}_0}V + V\frac{1}{\varepsilon - \mathcal{H}_0}V\frac{1}{\varepsilon - \mathcal{H}_0}V + \cdots, \tag{3.1}$$

where V is the impurity potential given by a diagonal matrix, i.e.,

$$V = \begin{pmatrix} V(\boldsymbol{r}) & 0 \\ 0 & V(\boldsymbol{r}) \end{pmatrix}, \tag{3.2}$$

ε is the energy, and $\mathcal{H}_0 = \gamma\vec{\sigma}\cdot\boldsymbol{k}$ is the Hamiltonian in the absence of the potential. The $(p+1)$th order term of the T matrix is written as

$$\begin{aligned}(s, -\boldsymbol{k}|T^{(p+1)}|s, +\boldsymbol{k}) = {} & \frac{1}{LA}\sum_{s_1\boldsymbol{k}_1}\frac{1}{LA}\sum_{s_2\boldsymbol{k}_2}\cdots\frac{1}{LA}\sum_{s_p\boldsymbol{k}_p} \\ & \times \frac{V(-\boldsymbol{k}-\boldsymbol{k}_p)\cdots V(\boldsymbol{k}_2-\boldsymbol{k}_1)V(\boldsymbol{k}_1-\boldsymbol{k})}{[\varepsilon-\varepsilon_{s_p}(\boldsymbol{k}_p)]\cdots[\varepsilon-\varepsilon_{s_2}(\boldsymbol{k}_2)][\varepsilon-\varepsilon_{s_1}(\boldsymbol{k}_1)]} \\ & \times \mathrm{e}^{-\mathrm{i}\phi_s(-\boldsymbol{k})}(s|R[\theta(-\boldsymbol{k})]R^{-1}[\theta(\boldsymbol{k}_p)]|s_p) \\ & \times \cdots \times (s_2|R[\theta(\boldsymbol{k}_2)]R^{-1}[\theta(\boldsymbol{k}_1)]|s_1) \\ & \times (s_1|R[\theta(\boldsymbol{k}_1)]R^{-1}[\theta(\boldsymbol{k})]|s)\mathrm{e}^{i\phi_s(\boldsymbol{k})},\end{aligned} \tag{3.3}$$

where $V(\boldsymbol{k}_i - \boldsymbol{k}_j)$ is a Fourier transform of the impurity potential and phase factors $\exp[\mathrm{i}\phi_{s_j}(\boldsymbol{k}_j)]$ have been cancelled out for all the intermediate states $j = 1, \ldots, p$. Actually, we have $\theta(\boldsymbol{k}) = 0$ and $\theta(-\boldsymbol{k}) = +\pi$.

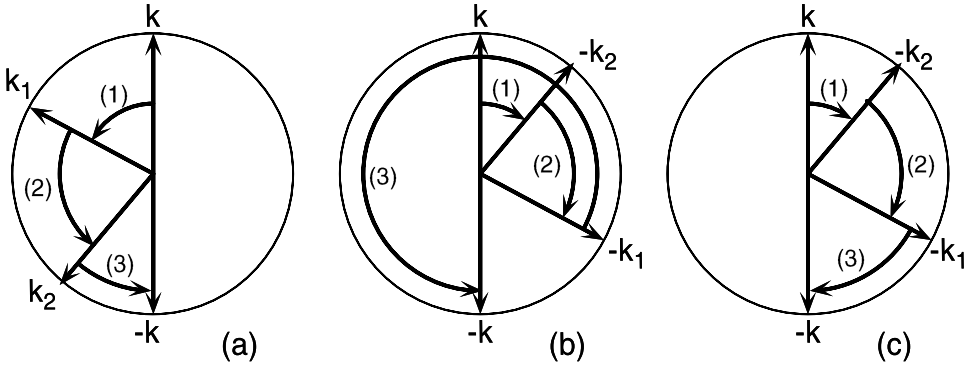

Fig. 2 Schematic illustration of the spin rotation corresponding to the scattering process $\boldsymbol{k} \to \boldsymbol{k}_1 \to \boldsymbol{k}_2 \to -\boldsymbol{k}$ (a) and its time-reversal process $\boldsymbol{k} \to -\boldsymbol{k}_2 \to -\boldsymbol{k}_1 \to -\boldsymbol{k}$. We have chosen $\theta(\boldsymbol{k}) = 0$ and $\theta(-\boldsymbol{k}) = +\pi$. In process (c), the final state is chosen as that obtained by $\theta(-\boldsymbol{k}) \to \theta(-\boldsymbol{k}) - 2\pi = -\pi$.

Define

$$\begin{aligned} S^{(p+1)} &= (s|R[\theta(-\boldsymbol{k})]R^{-1}[\theta(\boldsymbol{k}_p)]|s_p) \\ &\times \cdots \times (s_2|R[\theta(\boldsymbol{k}_2)]R^{-1}[\theta(\boldsymbol{k}_1)]|s_1) \\ &\times (s_1|R[\theta(\boldsymbol{k}_1)]R^{-1}[\theta(\boldsymbol{k})]|s). \end{aligned} \tag{3.4}$$

This quantity describes matrix elements of a rotation in the spin space and can be illustrated by a diagram as shown in Fig. 2(a). For each term in eq. (3.3), there is a term obtained through the replacement

$$(s_1, \boldsymbol{k}_1) \to (s_p, -\boldsymbol{k}_p), \quad (s_2, \boldsymbol{k}_2) \to (s_{p-1}, -\boldsymbol{k}_{p-1}), \quad \text{etc.}, \tag{3.5}$$

corresponding to the electron motion of a time-reversal path (see Fig. 3). Both matrix elements of the impurity potential and energy denominators remain unchanged by this replacement in eq. (3.3) except that S should be replaced by S' given by

$$\begin{aligned} S^{(p+1)\prime} =& (s|R[\theta(-\boldsymbol{k})]R^{-1}[\theta(-\boldsymbol{k}_1)]|s_1) \\ &\times \cdots \times (s_{p-1}|R[\theta(-\boldsymbol{k}_{p-1})]R^{-1}[\theta(-\boldsymbol{k}_p)]|s_p) \\ &\times (s_p|R[\theta(-\boldsymbol{k}_p)]R^{-1}[\theta(\boldsymbol{k})]|s). \end{aligned} \tag{3.6}$$

This process is given by a diagram as shown in Fig. 2(b). Instead of the above we consider the quantity $S^{(p+1)\prime\prime}$ given by

$$\begin{aligned} S^{(p+1)\prime\prime} =& (s|R[\theta(-\boldsymbol{k}) - 2\pi]R^{-1}[\theta(-\boldsymbol{k}_1)]|s_1) \\ &\times \cdots \times (s_{p-1}|R[\theta(-\boldsymbol{k}_{p-1})]R^{-1}[\theta(-\boldsymbol{k}_p)]|s_p) \\ &\times (s_p|R[\theta(-\boldsymbol{k}_p)]R^{-1}[\theta(\boldsymbol{k})]|s), \end{aligned} \tag{3.7}$$

which has been obtained from eq. (3.6) through the replacement $\theta(-\boldsymbol{k}) \to \theta(-\boldsymbol{k}) - 2\pi$ and can be represented by a diagram shown in Fig. 2(c). Using eq. (2.9), we have $S^{(p+1)\prime\prime} = -S^{(p+1)\prime}$. According to the present definition of the angle given by eq. (2.10), we have

$$\theta(-\boldsymbol{k}_j) = \begin{cases} \theta(\boldsymbol{k}_j) - \pi & \text{if} \quad \theta(\boldsymbol{k}_j) > 0\ , \\ \theta(\boldsymbol{k}_j) + \pi & \text{if} \quad \theta(\boldsymbol{k}_j) \le 0\ . \end{cases} \tag{3.8}$$

However, we can always put $\theta(-\boldsymbol{k}_j) = \theta(\boldsymbol{k}_j) - \pi$ for $j = 1, \ldots, p$ in the expression of $S^{(p+1)\prime\prime}$ because of eq. (2.9) since $\theta(-\boldsymbol{k}_j)$ always appears in a pair. By making the replacement $\theta(\boldsymbol{k}) \to \theta(-\boldsymbol{k}) - \pi$ and $\theta(-\boldsymbol{k}) \to \theta(\boldsymbol{k}) + \pi$, we can immediately obtain

$$S^{(p+1)\prime\prime} = -S^{(p+1)\prime} = S^{(p+1)*}. \tag{3.9}$$

More explicitly, we have

$$(s|R(\theta)R^{-1}(\theta')|s') = \begin{cases} \cos[(\theta - \theta')/2] & (s = s'), \\ -\mathrm{i}\sin[(\theta - \theta')/2] & (s \neq s'), \end{cases} \tag{3.10}$$

which is either real or pure imaginary. Because the number of matrix elements for different bands is always even in the expression of $S^{(p+1)}$, we see immediately that $S^{(p+1)}$ is given by a real number. Therefore, we have

$$S^{(p+1)\prime\prime} = -S^{(p+1)\prime} = S^{(p+1)}, \tag{3.11}$$

which shows that each term is canceled by the contribution of a corresponding time-reversal process in eq. (3.3). Further, the origin of the cancellation can be traced back to eq. (2.9), i.e., the fact that a rotation in the spin space by 2π gives rise to a sign change in the wave function.

The above discussion shows that each scattering process is described by a corresponding spin rotation. This is a direct consequence of the fact that a neutrino described by Weyl's equation (2.1) has a helicity, i.e., its spin is always in the direction of its wave vector. However, although states of 2D graphite in the vicinity of the Fermi level are formally described by Weyl's equation, two components of the wave function do not describe states of the actual electron spin but correspond only to the amplitude at two carbon sites in a unit cell. Even in this case the rotation of the wave vector around the origin gives rise to the same signature change. This can be directly obtained as a Berry's phase.[35,36]

Consider a wave function given by

$$\psi_s(\boldsymbol{k}) = \frac{1}{\sqrt{2}} \begin{pmatrix} -\mathrm{i}s \\ \exp[\mathrm{i}\theta(\boldsymbol{k})] \end{pmatrix}. \tag{3.12}$$

This is the "spin" part of an eigenfunction of the $\boldsymbol{k}\cdot\boldsymbol{p}$ equation, obtained by choosing $\phi_s(\boldsymbol{k}) = \theta(\boldsymbol{k})/2$ in such a way that the wave function becomes continuous as a function of $\theta(\boldsymbol{k})$.[37] When the wave vector $\boldsymbol{k}$ is rotated in the anticlockwise direction adiabatically as a function

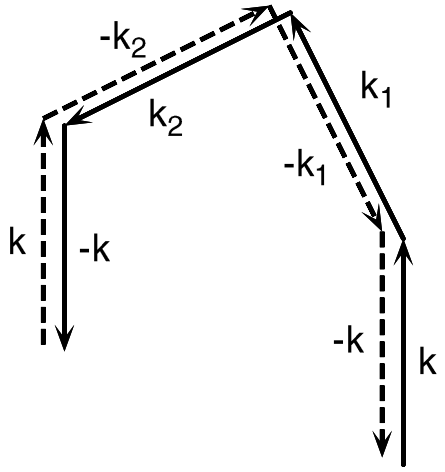

Fig. 3 Schematic illustration of a back scattering process (solid arrows) and corresponding time-reversal process (dashed arrows).

of time t around the origin for a time interval $0<t<T$, the wavefunction is changed into $\psi_s(\boldsymbol{k})\exp(-\mathrm{i}\varphi)$, where φ is Berry's phase given by

$$\varphi = -\mathrm{i}\int_0^T \mathrm{d}t \left\langle \psi_s[\boldsymbol{k}(t)] \middle| \frac{\mathrm{d}}{\mathrm{d}t}\psi_s[\boldsymbol{k}(t)] \right\rangle = \pi. \qquad (3.13)$$

This shows that the rotation in the $\boldsymbol{k}$ space by 2π leads to the change in the phase by $+\pi$, i.e., a sign change. Note that $R^{-1}[\theta(\boldsymbol{k})]|s)$ is obtained from eq. (3.12) by continuously varying the direction of $\boldsymbol{k}$ including Berry's phase.

A similar phase change of the back scattering process is the origin of the so-called anti-localization effect in systems with strong spin-orbit scattering.[38] In the absence of spin-orbit interactions, the scattering amplitude of each process and that of corresponding time-reversal process are equal and therefore their constructive interference leads to an enhancement in the amplitude of back scattering processes. This gives rise to the so-called quantum correction to the conductivity in the weak localization theory.[39] In the presence of a strong spin-orbit scattering, however, scattering from an impurity causes a spin rotation and resulting phase change of the wave function leads to a destructive interference. As a result the quantum correction has a sign opposite to that in the absence of a spin-orbit scattering.[40] This anti-localization effect was observed experimentally.[41,42]

§4. Higher Order Effective-Mass Equation

The absence of back scattering can be destroyed by various effects. When the potential range becomes shorter than the lattice constant, the back scattering appears because of two reasons as was shown previously.[2] The first is that the effective potential of an impurity for A and B sites can be different. This causes mixing of the spin space and the momentum space and the resulting "spin-orbit" interaction makes the back-scattering probability nonzero. The second, which is more important, is the appearance of inter-valley matrix elements between K and K' points.

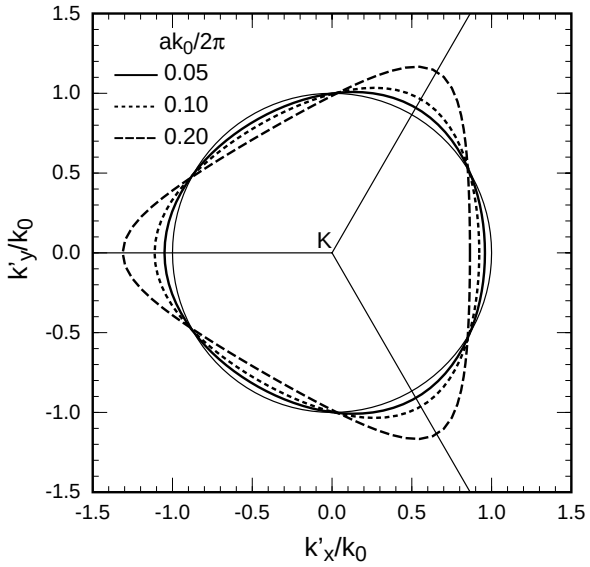

Fig. 4 Some examples of equi-energy lines in the vicinity of the K point. The trigonal warping increases with $ak_0/2\pi$ where k_0 is the magnitude of the wave vector corresponding to the energy obtained by neglecting higher order terms. The k'_x and k'_y directions are fixed onto the graphite sheet.

As another example we shall consider effects of higher order $\boldsymbol{k}\cdot\boldsymbol{p}$ terms. A higher order $\boldsymbol{k}\cdot\boldsymbol{p}$ equation was derived already in a simple tight-binding model including only a π orbital for each carbon atom as[15]

$$\begin{pmatrix} 0 & \gamma\left[(\hat{k}_x-\mathrm{i}\hat{k}_y)+\dfrac{a\mathrm{e}^{3\mathrm{i}\eta}}{4\sqrt{3}}(\hat{k}_x+\mathrm{i}\hat{k}_y)^2\right] \\ \gamma\left[(\hat{k}_x+\mathrm{i}\hat{k}_y)+\dfrac{a\mathrm{e}^{-3\mathrm{i}\eta}}{4\sqrt{3}}(\hat{k}_x-\mathrm{i}\hat{k}_y)^2\right] & 0 \end{pmatrix}\begin{pmatrix} F_A \\ F_B \end{pmatrix} = \varepsilon \begin{pmatrix} F_A \\ F_B \end{pmatrix}, \qquad (4.1)$$

for the K point, where η is the chiral angle. This gives trigonal warping of the band around the K point. In fact, the energy bands are given in the lowest order of $a|\boldsymbol{k}|$ by

$$\varepsilon_s(\boldsymbol{k}) = s\gamma|\boldsymbol{k}| + \Delta\varepsilon_s(\boldsymbol{k}), \qquad (4.2)$$

with

$$\Delta\varepsilon_s(\boldsymbol{k}) = s\gamma|\boldsymbol{k}|\frac{a|\boldsymbol{k}|}{4\sqrt{3}}\sin[3(\theta+\eta)], \qquad (4.3)$$

where $\theta=\theta(\boldsymbol{k})$. Figure 4 gives some examples of equi-energy lines for various values of $ak_0/2\pi$ with $\varepsilon = s\gamma k_0$. The corresponding results for the K' point are obtained by rotating those for the K point by $\pi/3$.

The wave function of the state corresponding to wave vector $\boldsymbol{k}=(k_x,k_y)$ is given by eqs. (2.3) and (2.5), where $\theta(\boldsymbol{k})$ is replaced by

$$\tilde{\theta}(\boldsymbol{k}) = \theta(\boldsymbol{k}) + \Delta\theta(\boldsymbol{k}), \qquad (4.4)$$

with

$$\Delta\theta(\boldsymbol{k}) = -\frac{a|\boldsymbol{k}|}{4\sqrt{3}}\cos[3(\theta+\eta)]. \qquad (4.5)$$

For a given energy $\varepsilon = s\gamma k_0$ ($\varepsilon>0$ and $k_0>0$), the wave

vector in the y direction for $k_x=0$ changes from $+k_0$ into $k_+=k_0+\Delta k_+$ and from $-k_0$ into $k_-=-k_0+\Delta k_-$ with

$$\Delta k_+ = \Delta k_- = -\frac{ak_0^2}{4\sqrt{3}}\sin 3\eta. \tag{4.6}$$

These expressions are correct to the order in $a|\boldsymbol{k}|$ or ak_0.

The matrix element of the potential $V(\boldsymbol{r})$ corresponding to scattering from a state $\boldsymbol{k}_+ = (0, k_+)$ to $\boldsymbol{k}_- = (0, k_-)$ is calculated as

$$\begin{aligned} &\mathrm{e}^{\mathrm{i}[\phi_s(\boldsymbol{k}_+)-\phi_s(\boldsymbol{k}_-)]}\frac{V(-2k_0)}{AL}(s|R[\tilde{\theta}(\boldsymbol{k}_-)]R^{-1}[\tilde{\theta}(\boldsymbol{k}_+)]|s) \\ =&\mathrm{e}^{\mathrm{i}[\phi_s(\boldsymbol{k}_+)-\phi_s(\boldsymbol{k}_-)]}\frac{V(-2k_0)}{AL}\frac{ak_0}{4\sqrt{3}}\cos 3\eta, \end{aligned} \tag{4.7}$$

in the lowest order with respect to ak_0, where

$$V(-2k_0) = \int dx \int dy\, V(\boldsymbol{r})\exp(2\mathrm{i}k_0 y). \tag{4.8}$$

The result shows that in the lowest order Born approximation the back scattering probability is proportional to

$$(k_0 a)^2\cos^2 3\eta\,|V(-2k_0)|^2, \tag{4.9}$$

which increases in proportion to ε^2 except in the case of $\eta=\pi/6$ (armchair CN).

When $\eta=\pi/6$, the wave vector in the axis direction is modified by higher order terms most strongly as shown in eq. (4.6) and in Fig. 4, while the wave function remains as eqs. (2.3) and (2.5) because $\Delta\theta(\boldsymbol{k}_+)=\Delta\theta(\boldsymbol{k}_-)=0$. The "spin" part of the wave function for $\boldsymbol{k}_+$ and $\boldsymbol{k}_-$ are orthogonal to each other, which leads to the vanishing back scattering probability. This is a direct consequence of the symmetry of the energy bands under the mirror reflection $k_x\to -k_x$. In other cases, the phase of the wave functions for states with $\boldsymbol{k}_+$ and $\boldsymbol{k}_-$ changes in a different way and the resulting phase difference proportional to $k_0 a\cos 3\eta$ gives rise to the nonvanishing back-scattering probability.

More generally in armchair CN's, the effective-mass equation for $k_x=0$ is written as

$$\gamma\begin{pmatrix} 0 & -\frac{2\mathrm{i}}{a}\left[\sin\frac{\hat{k}a}{2}+\frac{1}{\sqrt{3}}\left(1-\cos\frac{\hat{k}a}{2}\right)\right] \\ \frac{2\mathrm{i}}{a}\left[\sin\frac{\hat{k}a}{2}+\frac{1}{\sqrt{3}}\left(1-\cos\frac{\hat{k}a}{2}\right)\right] & 0 \end{pmatrix}\begin{pmatrix}F_A\\F_B\end{pmatrix}=\varepsilon\begin{pmatrix}F_A\\F_B\end{pmatrix}, \tag{4.10}$$

with $\hat{k}$ being the wave vector operator in the y direction. This shows that the eigenfunction remains the same and that the back scattering probability vanishes in the lowest order Born approximation even if further higher order $\boldsymbol{k}\cdot\boldsymbol{p}$ terms are included.

It is highly likely that the back scattering has a nonzero probability when terms in higher orders in the external potential are included, i.e., in a higher order Born approximation, even at $k=0$ and also in armchair nanotubes. In fact, in previous sections the use has been made of the fact $\varepsilon_s(-\boldsymbol{k})=\varepsilon_s(\boldsymbol{k})$ explicitly in showing the exact cancellation of a term in the T matrix with a term corresponding to a time reversal process. The inversion symmetry of the energy band is destroyed by the trigonal warping and the discussion there becomes no longer valid. This is expected to cause a small back scattering probability unless some other mechanisms of cancellations are still present.

Consider, for example, an armchair nanotube and an external potential which is symmetric under a mirror reflection with respect to a line parallel to the axis. In this case we can use the symmetry of the energy bands under the mirror reflection $k_x\to -k_x$ to show vanishing back scattering probability. In fact, each term in the T matrix can be shown to be cancelled by a term in which $\boldsymbol{k}_j=(k_x^j, k_y^j)$ for intermediate states $j=1,\ldots,p$ is replaced by $\bar{\boldsymbol{k}}_j=(-k_x^j, k_y^j)$.

§5. Discussion and Conclusion

The absence of back scattering $\boldsymbol{k}\to -\boldsymbol{k}$ has been shown to be related to the well-known sign change of an electron spin under a rotation of angle 2π. This is nothing but a Berry's phase acquired by a rotation of the wave vector in the system described by a degenerate $\boldsymbol{k}\cdot\boldsymbol{p}$ Hamiltonian arising from the presence of two carbon atoms in a unit cell. Effects of trigonal warping of the bands appearing in a higher order $\boldsymbol{k}\cdot\boldsymbol{p}$ approximation have been shown to give rise to a small but nonzero probability of back scattering.

Most of the results given so far are expected to be valid for scattering from dynamical perturbations such as lattice vibrations. In fact, at sufficiently low temperatures, only long wavelength acoustic phonons are excited and their effects can be incorporated as a deformation potential given by a diagonal matrix in the $\boldsymbol{k}\cdot\boldsymbol{p}$ scheme. This immediately leads to the vanishing back scattering at least in the lowest Born approximation. At high temperatures, however, optical phonons may give rise to nonzero back scattering probability through inter-valley scattering between K and K' points. A similar conclusion can be reached also for mutual electron-electron scattering. These problems are left for a future study.

The present results have been obtained under the assumption that the energy bands of CN's can be reproduced by introducing periodic boundary conditions in the circumference direction into the energy bands of a 2D graphite sheet. Actually we have to consider mixing of the π bands with σ and other higher-lying bands due to the presence of a finite curvature particularly in CN's having a small circumference. This mixing is likely to cause a small but nonzero back scattering probability. Such effects of a finite curvature are interesting but also left for a future study.

The absence of back scattering can lead to an extremely large conductivity in carbon nanotubes. As was shown previously,[2] this effect disappears in magnetic fields, which is likely to give rise to a huge positive magnetoresistance. The conductance of a single-wall nan-

otube was observed quite recently,[43,44] but experiments show large charging effects presumably due to nonideal contacts. It is highly desirable to become able to measure transport of a single-wall nanotube with ideal Ohmic contacts.

Acknowledgments

This work was supported in part by Grant-in-Aid for Scientific Research from Ministry of Education, Science and Culture.

1) S. Iijima: Nature (London) **354** (1991) 56.
2) T. Ando and T. Nakanishi, J. Phys. Soc. Jpn. **67** (1998) No. 5.
3) N. Hamada, S. Sawada, and A. Oshiyama: Phys. Rev. Lett. **68** (1992) 1579.
4) J. W. Mintmire, B. I. Dunlap, and C. T. White, Phys. Rev. Lett. **68** (1992) 631.
5) R. Saito, M. Fujita, G. Dresselhaus, and M. S. Dresselhaus: Phys. Rev. B **46** (1992) 1804.
6) R. Saito, M. Fujita, G. Dresselhaus, and M. S. Dresselhaus: Appl. Phys. Lett. **60** (1992) 2204.
7) M. S. Dresselhaus, G. Dresselhaus, and R. Saito: Phys. Rev. B **45** (1992) 6234.
8) M. S. Dresselhaus, G. Dresselhaus, R. Saito, and P. C. Eklund: *Elementary Excitations in Solids*, ed. J. L. Birman, C. Sebenne, and R. F. Wallis (Elsevier Science Publishers B.V., Amsterdam, 1992) p. 387.
9) R. A. Jishi, M. S. Dresselhaus, and G. Dresselhaus: Phys. Rev. B **47** (1993) 16671.
10) K. Tanaka, K. Okahara, M. Okada, and T. Yamabe: Chem. Phys. Lett. **191** (1992) 469.
11) Y. D. Gao and W. C. Herndon: Mol. Phys. **77** (1992) 585.
12) D. H. Robertson, D. W. Berenner, and J. W. Mintmire: Phys. Rev. B **45** (1992) 12592.
13) C. T. White, D. C. Robertson, and J. W. Mintmire: Phys. Rev. B **47** (1993) 5485.
14) H. Ajiki and T. Ando: J. Phys. Soc. Jpn. **62** (1993) 1255.
15) H. Ajiki and T. Ando: J. Phys. Soc. Jpn. **65** (1996) 505.
16) H. Ajiki and T. Ando: J. Phys. Soc. Jpn. **62** (1993) 2470; *ibid* **64** (1995) 260.
17) H. Ajiki and T. Ando: J. Phys. Soc. Jpn. **64** (1995) 4382.
18) H. Ajiki and T. Ando: Physica B **201** (1994) 349.
19) H. Ajiki and T. Ando: Jpn. J. Appl. Phys. Suppl. **34** (1995) 107.
20) T. Ando: J. Phys. Soc. Jpn. **66** (1997) 1066.
21) N. A. Viet, H. Ajiki, and T. Ando: J. Phys. Soc. Jpn. **63** (1994) 3036.
22) H. Ajiki and T. Ando: J. Phys. Soc. Jpn. **64** (1995) 260.
23) S. N. Song, X. K. Wang, R. P. H. Chang, and J. B. Ketterson: Phys. Rev. Lett. **72** (1994) 697.
24) L. Langer, V. Bayot, E. Grive, J. -P. Issi, J. P. Heremans, C. H. Olk, L. Stockman, C. Van Haesendonck, and Y. Brunseraede: Phys. Rev. Lett. **76** (1996) 479.
25) F. Katayama: Master thesis (Univ. Tokyo, 1996).
26) W. -D. Tian and S. Datta: Phys. Rev. B **49** (1994) 5097.
27) R. Saito, G. Dresselhaus, and M. S. Dresselhaus: Phys. Rev. B **53** (1996) 2044.
28) R. Tamura and M. Tsukada: Solid State Commun. **101** (1997) 601.
29) R. Tamura and M. Tsukada: Phys. Rev. B **55** (1997) 4991.
30) T. Nakanishi and T. Ando: J. Phys. Soc. Jpn. **66** (1997) 2973.
31) Y. Miyamoto, S. G. Louie, and M. L. Cohen, Phys. Rev. Lett. **76** (1996) 2121.
32) T. Seri and T. Ando: J. Phys. Soc. Jpn. **66** (1997) 169.
33) T. Ando and T. Seri: J. Phys. Soc. Jpn. **66** (1997) 3558.
34) J. C. Slonczewski and P. R. Weiss: Phys. Rev. **109** (1958) 272.
35) M. V. Berry: Proc. Roy. Soc. London **A392** (1984) 45.
36) B. Simon: Phys. Rev. Lett. **51** (1983) 2167.
37) N. H. Shon and T. Ando: J. Phys. Soc. Jpn. **67** (1998) No. 7.
38) S. Hikami, A. I. Larkin, and Y. Nagaoka, Prog. Theor. Phys. **63** (1980) 707.
39) *Anderson Localization*, edited by Y. Nagaoka and H. Fukuyama (Springer, Berlin, 1982); *Localization, Interaction, and Transport Phenomena*, edited by B. Kramer, G. Bergmann, and Y. Bruynseraede (Springer, Berlin, 1984); P. A. Lee and T. V. Ramakrishnan: Rev. Mod. Phys. **57** (1985) 287; *Anderson Localization*, edited by T. Ando and H. Fukuyama (Springer, Berlin, 1988); D. J. Thouless: Phys. Reports C **13** (1974) 93.
40) G. Bergmann: Phys. Rept. **107** (1984) 1.
41) F. Komori, S. Kobayashi, and W. Sasaki: J. Phys. Soc. Jpn. **51** (1982) 3162.
42) G. Bergmann: Phys. Rev. Lett. **48** (1982) 1046.
43) S. J. Tans, M. H. Devoret, H. -J. Dai, A. Thess, R. E. Smalley, L. J. Geerligs, and C. Dekker: Nature **386** (1997) 474.
44) M. Bockrath, D. H. Cobden, P. L. McEuen, N. G. Chopra, A. Zettl, A. Thess, and R. E. Smalley: Science **275** (1997) 1922.